Transactions of the **14th International Conference on Structural Mechanics in Reactor Technology** (SMiRT 14), Lyon, France, August 17-22, 1997 **P03/6**

Stability evaluation of PWR containment steel liner for given flaws by use of 2D and 3D FEM computation

David O.(1), Humbert J.M.(1), Duval C.(2)
(1) CEA, France
(2) EDF, France

Abstract

The leaktightness prediction of PWR containment steel liners requires to be able to describe the influence of initial flaws such as broken studs and shape flaws. The use of 3D finite element large displacement calculations allows the evaluation of strain concentration generated by buckling phenomena. Such calculations on a representative section of a containment leads to limited strain concentrations for given initial flaws.

1 Introduction

This article is dedicated to a methodology for evaluating the leaktightness of the PWR containment steel liners in case of coupled thermal and pressure spikes.
Many important studies have been performed in the past [1, 2] to evaluate the performance of containment buildings under severe accident conditions. Liner tearing appeared then as a potential loss of integrity risk by the safety authorities.
In our contribution, we concentrate on the way to evaluate the influence of initial flaws such as a broken stud, a weak weld or shape flaw. We consider a representative section of a containment. It is composed of welded metal panels fixed to a prestressed and reinforced concrete containment by means of studs and angle bars (fig 1).
For the purpous of this prospective study, the loadings are represented by a theoritical steady increase of pressure and temperature beyond the design requirements (fig. 2).
The mechanical analysis is composed of:

- Thermal transient computation to evaluate the temperatures inside the liner and concrete.
- 2D axisymetrical mechanical computations to obtain the displacements fields of the studs, the angle bars and of the concrete.
- 3D large displacement computations to evaluate the strain concentration after buckling when an initial flaw is present.

The computations were made using CASTEM 2000 [3] an F.E. code developed by CEA-DMT-SEMT.

2 Thermal transient calculations

2.1 One dimensional modelling

This model takes into account the conduction through a $6mm$ thick steel sheet (the liner) and a concrete block whose thickness is equivalent to that of the containment ($0.9m$ in our case). Two convection boundary conditions are applied on both sides of the model with two given temperatures. On the liner side, this temperature follows that of the bulk containment atmosphere as described in figure 2. On the concrete side, the given temperature is fixed at $20°C$. The thermal conductivities used for the computations are those usually taken for steel and concrete. To take into account of the steam condensation on the steel panels, the exchange coefficient between the liner and the atmosphere is set at $100Wm^{-2}K^{-1}$. On the concrete side, it is set at $16Wm^{-2}K^{-1}$.

2.2 Results

Due to the exchange coefficient value on the liner side, the results of the thermal calculations show a small delay in the heating of the liner. While it takes $20s$ for the atmosphere to be heated to $140°C$ (fig 2), the liner reaches $120°C$ in $20min$. From one hour after the begining of the accident to the end, the difference between the containment atmosphere's temperature and the liner becomes negligible. Figure 3 shows the temperature through the concrete for selected time steps. We can see, that it takes four days, for this kind of accident, to have a linear temperature gradient through the concrete and that the cooling of the atmosphere at the end of the scenario causes an inversion of this gradient.
The temperature fields computed with this model will be used as input data in the 2D axially symmetrical mechanical model of the the containment.

3 2D Mechanichal evaluations

3.1 Mechanical modelling

The 2D model (fig 4) is for a representative section of the containment. This means, the liner and its anchorages (studs), the reinforcing bars and angles, the prestressing cables and the concrete. The liner is modelled with thin shell elements. The vertical reinforcing bars and angles and the vertical prestressing cables are modelled with 1D thin shell elements. The hoop rebars and prestressing cables are modelled with hoop elements. The concrete is modelled with 4-node quadrilateral elements.

3.2 Material behaviour

All the metal parts follow an elastoplastic mechanical behaviour with isotropic hardening. The yield criterion is the Von-Mises stress. The concrete follows the Ottosen mechanical behaviour [4]. This behaviour takes into account the cracks and softening in the material.

We can summarize the material properties as follow (where E is Young's modulus, ν Poisson's ratio, σ_e the yield strength and α the thermal expansion coefficient):

Liner	$: E = 2 \times 10^{11} Pa$	$\nu = 0.3$	$\sigma_e = 300 MPa$	$\alpha = 1.2 \times 10^{-5}\ ^oC^{-1}$
Concrete	$: E = 3 \times 10^{10} Pa$	$\nu = 0.2$	$\sigma_e = 4 MPa$	$\alpha = 1. \times 10^{-5}\ ^oC^{-1}$
Rebars	$: E = 2 \times 10^{11} Pa$	$\nu = 0.3$	$\sigma_e = 400 MPa$	$\alpha = 1.2 \times 10^{-5}\ ^oC^{-1}$
Cables	$: E = 2 \times 10^{11} Pa$	$\nu = 0.3$	$\sigma_e = 1500 MPa$	$\alpha = 1.2 \times 10^{-5}\ ^oC^{-1}$

3.3 Boundary conditions and loading

The boundary conditions of the model are those of an infinite cylinder (fig 4). The vertical displacements of the bottom of the concrete and the liner are set to zero. The vertical displacements of the whole upper surface of the concrete are equal. A unilateral relationship is used between the liner and the concrete. The liner is then joined to the concrete by the studs and angle bars which are embeded in the concrete, as are the reinforcing bars and the prestressing cables.
The variable loads applied on the sytem are the internal pressure and the thermal fields computed with the first model. The pressure is applied on the liner. The thermal field is 1D.
The constant loads on the representative section taken into account for the calculations are the weights of the structures, the prestress of the containment and the concrete's creeping and shrinkage. The latter were evaluated using the following empirical formulations:

$$\varepsilon_{creep} = 2 \times \varepsilon_{constantloads}$$
$$\varepsilon_{shrinkage} = 2 \times 10^{-4} \quad \text{where } \varepsilon \text{ is the average strain in the concrete}$$

The first step in the calculations loads the containment to its normal operating state. This means, the concrete is prestressed to withstand a $5 bars$ internal pressure. When this level is reached, the stress in the vertical cables is $1350 MPa$ and $1150 MPa$ in the hoop cables. The liner is in compression, close to its yield strength of $300 MPa$. These values allow us to evaluate the creep-strain as described above. After few iterations the system reaches an equilibrium state which is used as initial conditions.

3.4 Results. Cracking process in the concrete

The results of the 2D calculations show that the concrete starts cracking approximately 2.5 hours after the beginning of the accident as schown in figure 5. The first cracks appear at the hoop cables' location close to the external side. Fig. 3 shows that for this time, the internal side of the concrete has already reached the temperature of $80°C$. The internal pressure in the containment at this time is close to $5 bars$. Under its effect, the stresses in the concrete are close to zero in all directions (prestress compensation). The thermal field in the concrete will create a bending effect that causes the internal side to be in compression, and the external side to be in tension. This is why the concrete starts cracking on the external side. We can see that on the extrados (figure 5), the stresses in the vertical and in the hoop direction increase at the same rate from nearly zero to the rupture stress. At the same time, the intrados starts being compressed. As the thermal strain

of the concrete increases on the extrados, the concrete starts softening and the stresses decrease until they reach zero. To maintain the equilibrium in the structure, the stresses on the intrados start decreasing at the same time. After 4 hours, the concrete is cracked over two thirds of its thickness. As the internal pressure is still increasing, before reaching the $10bars$ value at 2 days, we can see that the stresses on the intrados also increase. The rate stress increase is higher in the hoop direction than in the vertical direction. For this reason we can assume that the cracks on the intrados are caused by the effect of the pressure instead of that of the thermal field which would have produced an equivalent rate of increase the two directions. There is no further evolution of the crack field after 2 days.

3.5 Results. Deformation of the liner

Under the effect of pressure, the stresses in the liner whose initial load was close to $-300MPa$, start increasing (prestresss compensation. fig 6). Its temperature increases faster than that of the concrete. The concrete's stiffeness is much higher than that of the liner and the liner's expansion will then be blocked by the concrete. When its temperature is high enough, the liner starts yielding in compression, reaching an equivalent plastic strain of $\varepsilon_{plastic} = 2.2 \times 10^{-3}$ After this yielding phase, as the pressure in the containment and the temperature of the concrete increase, the load on the liner increases. Close to the pressure peak ($10bars$ at 2 days), the liner starts yielding in tension, but there is no further yielding after this time. The final maximum equivalent plastic strain is of $\varepsilon_{plastic} = 3.6 \times 10^{-3}$.

4 3D Mechanical calculations

4.1 Modelling, boundary conditions and loadings

To evaluate the buckling of the liner and the strain concentrations, a 3D thin shell model of one fourth of a liner panel was made (fig 7). A projection of the displacements of the studs heads and the angle bars computed with the 2^{nd} model is used as an imposed displacement condition at the studs and angles locations. A uniform temperature field is applied on the liner following the temperature computed with the thermal model. The internal pressure of the containment is applied on one side of the liner. On the other side, a unilateral displacement relationship between the panel and a virtual concrete is used to model the interaction between the liner and the containment. The study is made with the "large displacement" assumption which allows us to see the buckling of the panel under the loads applied.

4.2 Considered flaws

An initial shape flaw is given to the liner to initiate the phenomenon. The flaw is equivalent to the effect of an external pressure on the liner with an embedding boundary condition on the angle bars. The maximum displacement is then located at the centre of the panel. The value we set is $20mm$. By releasing the locks of selected studs (1 through 12 on figure 7) we are able to predict the behaviour of a panel with a flaw such as a broken stud or a weak weld and have an idea of the equivalent plastic strain and of a

possible strain concentration zone.
We present here the results for three configurations. The first is the reference case in which there are no broken studs and no weld flaw on the angle bar. In the second case the studs 1, 2, 3 and 4 (figure 7) were considered broken. In the third calculations, both the locks of the two angle bars are released. This means the displacement in the X direction of these boundaries is no longer imposed and simulates a weak weld.

4.3 Results

The calculations were made as long as the liner yields in compression.
Figure 8 shows the equivalent plastic strain field in the liner for our three configurations. For the reference case we can see that there is a light buckling of the structure on the centre of the panel. In this area, the equivalent plastic strain is of $\varepsilon_{plastic} = 2.5 \times 10^{-3}$. The higher values are located close to the first row (vertical) of studs. The plastic strain close to the second row of studs is also higher than in representative section of the model, but this area is highly localised. The average value in this section of the model is close to $\varepsilon_{plastic} = 2 \times 10^{-3}$. These values are in harmony with those found with the 2D model. In the second case (studs 1, 2, 3 and 4 broken), the results show a strain concentration close to stud 5. The maximum value is $\varepsilon_{plastic} = 1 \times 10^{-2}$. At the centre of the panel (upper left corner), we can see a blistering of the panel. The local equivalent plastic strain is here increased by bending effects. In the third case (locks of the two angle bars released) we can see that the maximum equivalent plastic strain is $\varepsilon_{plastic} = 4 \times 10^{-3}$. The location of the maximum strain is still close to the first row of studs. Some other configurations were studied: initial flaw of $2mm$ instead of $20mm$, one stud broken instead of four. In all these calculations the maximum equivalent plastic strain reached was not higher than $\varepsilon_{plastic} = 1.5 \times 10^{-2}$.

5 Conclusions

The Deformations of a containment's liner beyond design assumptions can be evaluated using three modelling phases; thermal 1D modelling to get the thermal loads, 2D mechanical elastoplastic computations to obtain the boundary mechanical loading of a liner panel, 3D large displacement calculation to get the strain concentrations in case of theoritical flaws.
This procedure allows to take into account the buckling phenomena. The influence of broken studs and of weld flaws can be checked and seem to lead to limited concentrations of deformation.

References

[1] W.A. von Riesemann, M.B. Parks. Current state of knowledge on the behaviour of steel liners in concrete containments subjected to overpressurization loads.
Nuclear Engineering and Design 157 (1995) 481-487

[2] M.B. Parks, D.S. Horschel, W.A. von Riesemann. Summary of NRC-Sponsored research on containment integrity
SMIRT 11 Transactions Vol. SDO (August 1991) Tokyo, Japan.

[3] P. Verpeaux, A. Millard, Th. Charras. CASTEM 2000, une approche moderne du calcul des structures
Calcul des structures et intelligence artificielle. Ed. Pluralis 1989.
[4] O. Dahlblom, N.S. Ottosen. Smeared crack analysis using generalized fictitious crak model.
Journal of Engineering Mechanics, Vol 16, January 1990

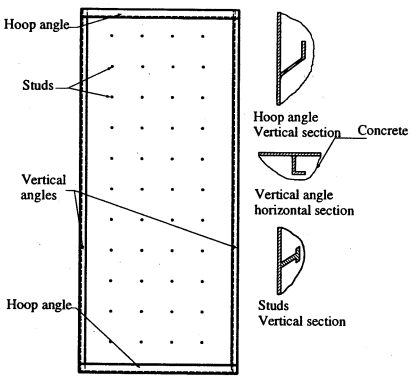

FIG. 1 – *Components design*

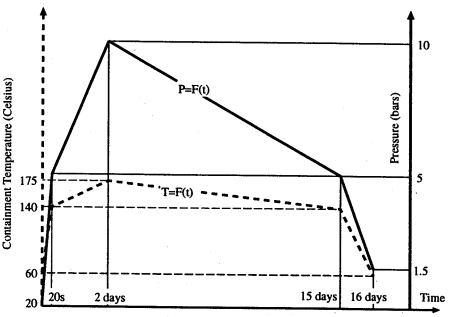

FIG. 2 – *Containment atmosphere temperature and pressure*

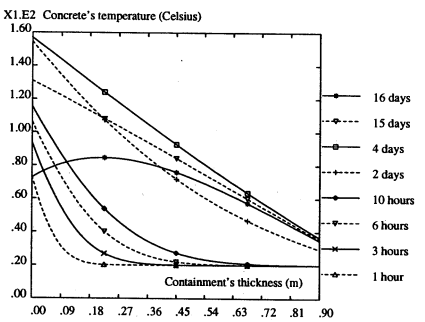

FIG. 3 – *Concrete temperature for selected times steps*

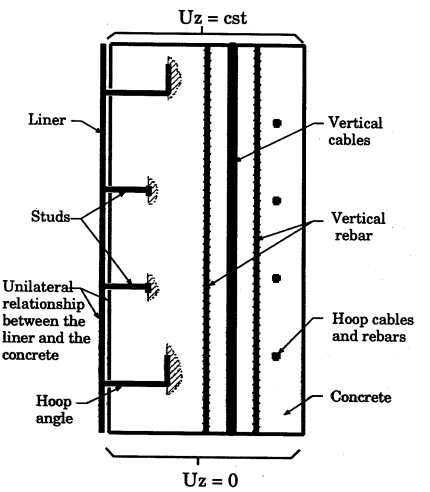

FIG. 4 – *Mechanical model*

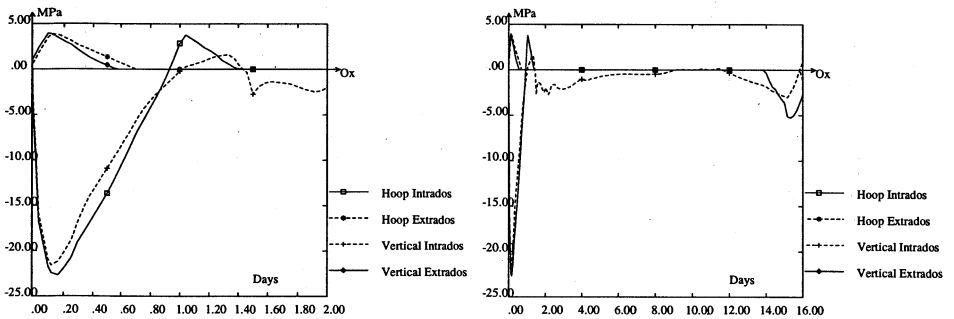

(a) 0 - 2 days (b) 0 - 16 days

FIG. 5 – *Stresses in the concrete*

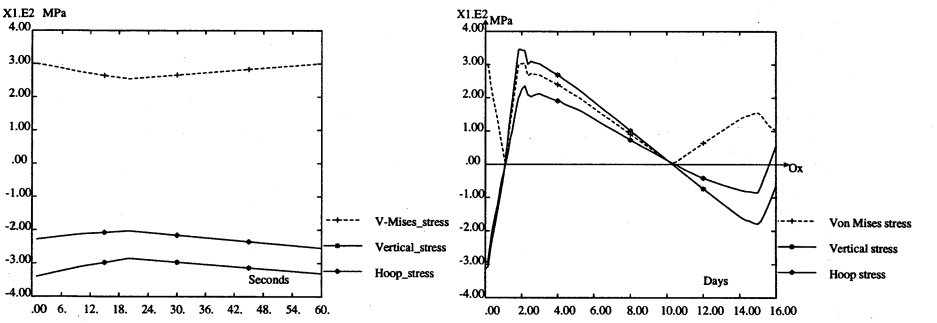

(a) 0 - 20 seconds (b) 0 - 16 days

FIG. 6 – *Stresses in the liner*

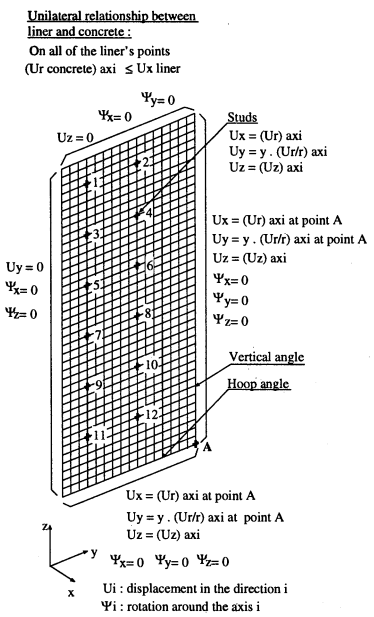

(a) Boundary conditions

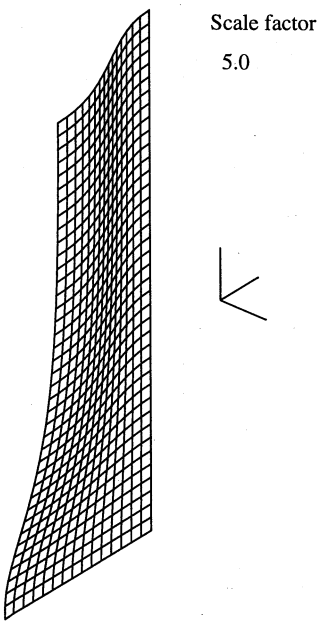

(b) Initial shape of the liner flaw

FIG. 7 – *3D Boundary conditions and initial shape of the assumed liner flaw*

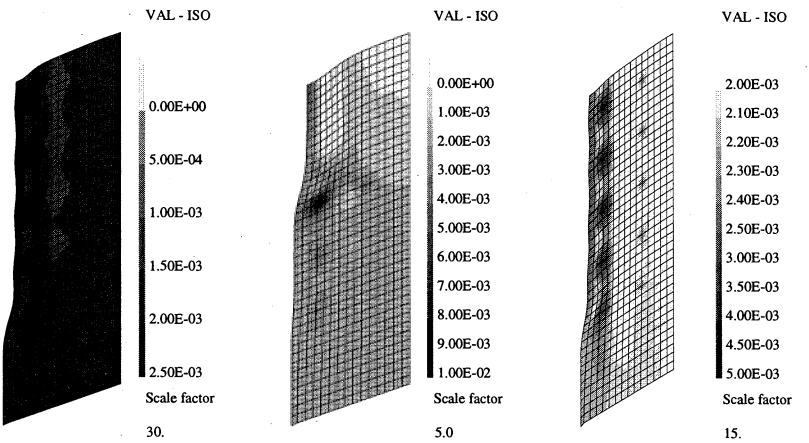

(a) Reference case (b) 4 broken studs (c) 2 broken angle bars

FIG. 8 – *Results of 3D calculations*